# Laser-Induced Desorption of CO from $Cr_2O_3$ (0001): Ab Initio Calculation of the Four-Dimensional Potential Energy Surface for an Intermediate Excited State

**Mikhail Pykavy,[†] Stephan Thiel,[‡] and Thorsten Klüner***

*Fritz-Haber-Institut der Max-Planck-Gesellschaft, Faradayweg 4-6, D-14195 Berlin, Germany*

*Received: July 24, 2002*

Ab initio cluster calculations for an excited state of the system CO/$Cr_2O_3$ (0001) are presented. A CO(a $^3\Pi$)-like state generated by an internal electronic excitation of the CO molecule ($5\sigma \rightarrow 2\pi^*$) is considered to be a possible intermediate for the laser-induced desorption of CO from $Cr_2O_3$ (0001). A four-dimensional potential energy surface (PES) for this state is calculated at the CASSCF level of theory. A few possible alternatives for the desorption intermediate are also discussed. The interaction mechanism between the excited CO molecule and the surface is analyzed, and it is shown that the change of symmetry of the quadrupole moment of the CO molecule is responsible for the topology of the calculated PES.

## 1. Introduction

The adsorption of the CO molecule on the $Cr_2O_3$ (0001) surface has been the subject for many experimental studies over the years.[1−6] It was found that the CO molecule adsorbs almost parallel to the surface. This is slightly surprising, because at metal oxide surfaces the CO molecule generally adsorbs perpendicular to the surface in the on-top position above the cation.[7] In our recent theoretical study of the ground state of the system CO/$Cr_2O_3$ (0001),[8] we could show that the unusual adsorption geometry is dominated by the interaction of the quadrupole moment of CO with the electric field gradient above the surface.

However, knowledge of the ground state alone is not sufficient to explain results of photoinduced desorption of CO from the $Cr_2O_3$ (0001) surface.[6] An analysis of the rotational alignment of the desorbing CO molecules exhibited a change of the rotational behavior as a function of the rotational quantum number *J*; at low *J*, the CO molecules desorb helicopter-like, while at large *J* values cartwheel-like rotation was found. To explain this stereodynamic effect, it was necessary to perform quantum dynamical calculations of the photodesorption process using information both for the ground state and for the excited state involved.[9]

Generally, the laser-induced desorption is initiated by an electronic transition (DIET, desorption-induced by electronic transitions) and is often discussed in qualitative one-dimensional (1D) scenarios such as the Menzel−Gomer−Redhead (MGR)[10,11] or the Antoniewicz[12] models. However, a realistic treatment of photodesorption requires a detailed knowledge of the multidimensional potential energy surfaces (PESs) involved. This is a notoriously difficult task since (i) all relevant degrees of freedom have to be considered in the construction of the PESs and (ii) PESs not only for the ground state but also for the electronically excited state are needed. To our knowledge, the only successful detailed theoretical study (two-dimensional (2D) ab initio PESs for the ground and excited states) has been performed for the NO/NiO (100) adsorbate−substrate system.[13]

In this study, we present an ab initio calculation of the four-dimensional (4D) PES for the excited state of the system CO/$Cr_2O_3$ (0001). Our calculation of a similar PES for the ground state of this adsorbate−substrate system was published and discussed elsewhere.[8] Recently, we have also reported a wave packet study in which the stereodynamic effects of CO desorbing from $Cr_2O_3$ (0001) could be explained.[9,14]

The first section of the present paper contains details of our theoretical model, the details of the quantum chemical calculations, and the fitting procedure. In the second part, we discuss the topology of the PES of the excited state and the interaction mechanism of the excited CO molecule with the surface. Conclusions and an outlook complete the paper.

## 2. Details of Modeling and Calculation

**2.1. Surface Structure.** Chromium oxide, α-$Cr_2O_3$, crystallizes in the well-known corundum structure,[15] which is a sequence of hcp oxygen layers with chromium ions occupying two-thirds of the available octahedral positions.

The $Cr_2O_3$ (0001) surface is terminated by a chromium layer, which contains only half of the chromium ions as compared to the bulk. The first interlayer distance between the uppermost chromium layer and the oxygen layer below undergoes a strong relaxation.[16−19] Because the exact extent of this relaxation is still not precisely known, we choose the theoretically predicted value of 40%[8,19] for our surface model. Small relaxations occur also in the deeper layers (up to the fifth ionic layer), but these relaxations do not influence the interaction of an adsorbed molecule with the surface.

Finally, there is a charge transfer between the chromium ions in the topmost surface layer and the oxygen ions in the layer below.[20] This leads to a partial reduction of the ionic charges in the first two layers of the surface from the nominal values +3 and −2 to +2.1 and −1.7 (for chromium and oxygen, respectively). The transferred electrons do not occupy the 3d shell of chromium, as one could expect, but form slightly covalent bonds between chromium and three adjacent oxygen

* To whom correspondence should be addressed. Tel: +49-30-8413-4219. Fax: +49-30-8413-4101. E-mail: kluener@fhi-berlin.mpg.de.

[†] Present address: Institut für Chemie, Sekretariat C3, Fakultät II, Technische Universität Berlin, Straβe des 17, Juni 135, D-10623 Berlin, Germany.

[‡] Present address: Max-Planck-Institut für Kohlenforschung, Kaiser-Wilhelm-Platz 1, D-45470 Mülheim an der Ruhr, Germany.

10.1021/jp026597h CCC: $22.00 
Published on Web 11/12/2002

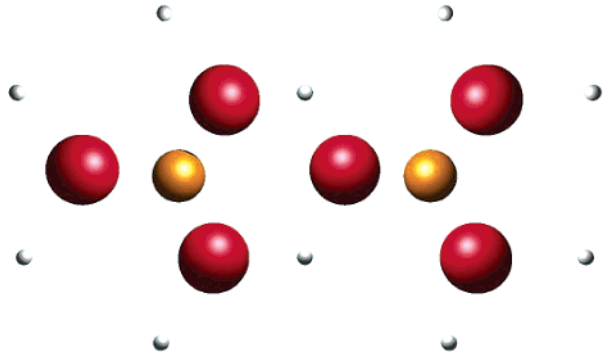

**Figure 1.** Top view of the $Cr_2O_6^{6-}$ cluster used to represent the $Cr_2O_3$ (0001) surface (O, large dark spheres; Cr, medium-sized gray spheres). Point charges that are adjacent to the oxygen atoms of the cluster were replaced by Al pseudopotentials (they are also shown by small bright spheres; the rest of the embedding point charges are not shown).

ions. Such charge transfer occurs only in the first two layers of the surface; the bulk remains strongly ionic. Thus, the $Cr_2O_3$ (0001) surface might be considered as a layer of quasi-covalent and flattened $CrO_3$ units distributed hexagonally on the ionic bulk with the original crystal structure.

**2.2. Surface Model.** The cluster model for the $Cr_2O_3$ (0001) surface was described in detail in our previous paper.[8] Only a brief description will be given here.

We use a small surface fragment containing two $CrO_3$ units as a $Cr_2O_6^{6-}$ cluster (Figure 1), which is embedded in a large point charge field (PCF). Point charges of +3 and −2 are used for Cr and O ions in the bulk and +2.1 and −1.7 for Cr and O at the surface. The PCF takes account of the long-range electrostatic potential above the surface. All positive point charges next to oxygen atoms of the cluster are replaced by effective core potentials in order to avoid an artificial polarization of the electron density at the oxygen ions toward the bare positive point charges. We have chosen Al cores because of the similarity between the corundum structures of both oxides $Al_2O_3$ and $Cr_2O_3$. It is however not essential which atoms are used to represent the repulsive cores.

The present surface model has been used successfully to describe the ground state of the $CO/Cr_2O_3$ (0001) system.[8] We have also found that the stoichiometric saturation of the cluster is of minor importance for the adsorption geometry and binding energy. Furthermore, the extension of the cluster in the lateral direction or into the bulk does not change the calculated binding energy. This is consistent with the fact that the surface consists of almost isolated $CrO_3$ units while the rest of the crystal is ionic. Just a few of such $CrO_3$ units are sufficient to model an adsorption site for a small molecule.

The position and orientation of the adsorbed CO molecule will be given using the following four coordinates (Figure 2): *Z*, the distance between the CO center of mass and the topmost Cr layer of the surface (bond distance); *X*, lateral displacement of the CO center of mass along a Cr−Cr line from the Cr on-top position; $\vartheta$, tilt angle that describes the orientation of the CO axis in the *XZ* plane (at $\vartheta = 0°$, the CO axis is perpendicular to the surface with the O end down); $\varphi$, the azimuthal angle, which describes the rotation of the CO axis in the surface plane *XY* (at $\varphi = 0°$, the CO molecule is in-line with the Cr−Cr line). These coordinates determine a 4D PES $f(X, Z, \vartheta, \varphi)$ for the adsorbed CO molecule. The remaining two degrees of freedom were frozen; (i) the lateral displacement along the *Y*-axis, i.e., out of the Cr−Cr line, is energetically very unfavorable and (ii) the CO bond distance was fixed at the experimental gas phase value $R_{CO} = 1.128$ Å.[21]

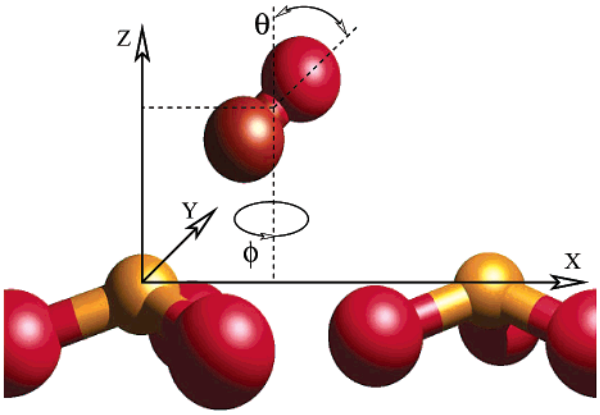


**Figure 2.** Coordinate system used to describe the position and the orientation of the adsorbed CO molecule.

**2.3. Nature of the Desorption Intermediate.** UV-laser irradiation of the adsorbate−substrate system may cause a series of different vibrational and electronic excitations in the substrate or adsorbate. We will restrict our study to pure electronic excitations, but there are various kinds of them: (i) charge transfer between the adsorbate and the substrate, (ii) internal surface excitations, and (iii) internal electronic excitations within the adsorbed molecules. Each of these electronic transitions may cause a DIET process. For instance, in a similar theoretical study of laser-induced desorption in the system NO/NiO (100),[13] it was proved that the formation of $NO^-$ as a result of charge transfer from the surface to the adsorbed NO molecule initiates the desorption.

However, an anionic desorption intermediate is unlikely for CO, because the CO anion is not stable in the gas phase (the electron affinity of CO is −1.33 eV[22]). However, a $CO^-$-like intermediate cannot be ruled out since a stabilization of the negative ion resonance might occur in the electric field above the polar $Cr_2O_3$ (0001) surface. For instance, a $CO^-$-like species has been found to be stable in the presence of F-centers.[23] Future studies will show whether a similar anion stabilization might be possible in the system $CO/Cr_2O_3$ (0001) as well.

It is even less likely that the CO molecule would transfer one electron to the surface since the ionization potential of CO is as high as 14.014 eV[24]. Thus, a charge transfer between substrate and adsorbate is unlikely in the desorption of CO from the $Cr_2O_3$ (0001) surface.

Internal surface transitions are unlikely as well. The nature of the bond between the CO molecule and the $Cr_2O_3$ (0001) surface has mainly electrostatic character[8] and would hardly change after d−d excitations within the chromium ions. Charge transfer within the surface (from oxygen to chromium) might lead to desorption. Such a charge transfer would cause the reduction of the ionic charges in the surface and, therefore, a decrease of the electrostatic forces acting on the adsorbed molecule. The extent of the charge reduction will be the same for both chromium ($+1e^-$) and oxygen ($-1e^-$) ions, so that the adsorbed molecule may simply lose the attraction to the surface and desorb. In this case, there is no obvious reason for CO to change its orientation. However, we have shown in our wave packet calculations[9,14] that the change of the CO orientation during the desorption is required for explaining of the experimental results concerning the stereodynamics of the CO desorption. Thus, we will not discuss the surface internal charge transfer as a possible desorption intermediate in the system $CO/Cr_2O_3$ (0001) any further.

Therefore, only an internal electronic excitation of the adsorbed CO molecule remains for the discussion of the

desorption mechanisms. The CO molecule possesses a X $^1\Sigma^+$ ground state with the electronic configuration ....$3\sigma^2 4\sigma^2 1\pi^4 5\sigma^2$. The excitation of one electron from $5\sigma$ to the lowest unoccupied $2\pi^*$ orbital gives rise to either the a $^3\Pi$ or the A $^1\Pi$ state with gas phase excitation energies of 6.0 and 8.1 eV, respectively.[21] Any of them might be involved in the desorption process, even though the transition $^1\Sigma^+ \rightarrow {}^3\Pi$ is spin forbidden (the normal selection rules are not necessarily applicable for the DIET intermediate, since indirect excitations mediated by electron hole pairs are possible as well). These singlet and triplet states differ only by the spin orientation of the unpaired electrons, so we expect a very similar interaction between the surface and an excited CO molecule in either state. (This will be discussed in the Sections 3.2 and 3.4 again.) We will consider the a $^3\Pi$ as a probable desorption intermediate and perform calculations of the corresponding 4D PES.

**2.4. Computational Methods and Basis Sets.** To describe the interaction of the nonexcited CO molecule with the $Cr_2O_6^{6-}$ cluster, we have mainly performed ROHF−SCF calculations (restricted open-shell Hartree−Fock self-consistent field) in our previous study.[8] This was possible because both interacting systems, the cluster and the CO molecule in their ground states, could be well-described by a single-reference wave function, and the interaction was mainly of electrostatic nature. Electron correlation effects have been found to be of minor importance for the adsorption energy and geometry.

The $Cr_2O_6^{6-}$ cluster contains two chromium ions, and each of them has three unpaired electrons in the 3d shell. The ground state of such an ion in the gas phase is a $^4$F state. In an octahedral surrounding, the 3d atomic orbitals split into $t_{2g}$ and $e_g$ orbitals. This gives rise for three terms, $^4T_{2g}$, $^4T_{1g}$, and $^4A_{2g}$, with different energies. The lowest term is the spatially nondegenerate $^4A_{2g}$ state, which corresponds to the 3d configuration $t_{2g}^3e_g^0$. At the surface, the ideal octahedral field is strongly modified. However, the ground state of each chromium ion remains a quartet state with three unpaired electrons in the three lowest 3d orbitals. Because of the large distance between the adjacent chromium ions at the surface ($a_0$ = 4.954 Å), the antiferromagnetic coupling is rather small[25] and can be neglected. Thus, we will consider only the ferromagnetic coupling of the unpaired electrons of the chromium ions in the cluster, i.e., we treat the $Cr_2O_6^{6-}$ cluster as a single-reference open-shell system in a high-spin septet state.

The a $^3\Pi$ state of CO, which we will consider as a DIET intermediate, is generated by excitation of one electron from the highest occupied $5\sigma$ orbital to the lowest unoccupied $2\pi^*$ orbital. To describe the 2-fold spatial degeneracy of this state correctly, we cannot use a single determinant approach (such as the Hartree−Fock SCF method) any more. Instead, we have to perform complete active space self-consistent field (CASSCF) calculations with an active space consisting of at least the $5\sigma$ and 2-fold degenerate $2\pi^*$ orbital of CO occupied by two electrons (CAS 3o:2e).

As noted above, the $Cr_2O_6^{6-}$ cluster contains two chromium ions with three unpaired 3d electrons each. Generally, we would have to consider all possible spin couplings between the unpaired electrons of the cluster and the CO molecule. However, as we will show in Section 3, in the regions of PES that are most important for the further wave packet dynamic calculations, the lowest state is always the one with the highest spin multiplicity. Thus, we can keep the unpaired electrons of the $Cr_2O_6^{6-}$ cluster with parallel spins (as we have also done for the ground state before).

**TABLE 1: Basis Sets for CO and $Cr_2O_6^{6-}$ Cluster Atoms**

| atom | standard basis set | smallest $\eta$ |
|---|---|---|
| | $Cr_2O_6^{6-}$ Cluster | |
| Cr | $(14s\ 9p\ 5d) \rightarrow \langle 9s\ 6p\ 4d\rangle$ of Wachters[32] | *s*: 0.038 |
| | augmented by *s* with $\eta = 0.24877$ | *p*: 0.494 |
| | | *d*: 0.347 |
| O | $(9s\ 5p) \rightarrow \langle 6s\ 3p\rangle$ of Huzinaga[31] | *s*: 0.289 |
| | | *p*: 0.215 |
| | CO Molecule | |
| C | $(9s\ 5p) \rightarrow \langle 6s\ 3p\rangle$ of Huzinaga[31] | *s*: 0.153 |
| | augmented by $2 \times d$ with $\eta = 1.0; 0.3$ | *p*: 0.115 |
| O | $(9s\ 5p) \rightarrow \langle 6s\ 3p\rangle$ of Huzinaga[31] | *s*: 0.289 |
| | augmented by $2 \times d$ with $\eta = 2.0; 0.5$ | *p*: 0.215 |

The resulting active space will contain the six singly occupied 3d orbitals at the two chromium ions of the cluster and the $5\sigma$ and $2\pi^*$ orbitals of the CO molecule. This active space is occupied by eight electrons (CAS 9o:8e). The states of interest are the two lowest nonet states, which correspond to the doubly degenerate $^3\Pi$ state of the CO molecule interacting with the $Cr_2O_6^{6-}$ cluster.

For each orientation ($\vartheta$, $\varphi$) of the CO* molecule at a given position *X* and bond distance *Z* above the surface, a state-averaged CASSCF calculation for two lowest $^9$A states was performed in order to optimize the orbitals. These orbitals were then used for subsequent valence configuration interaction (VCI) calculations with the same active space as for the CASSCF calculations ($5\sigma$, $2\pi^*$, $6 \times$ 3d of Cr with eight electrons, or VCI 9o:8e). In the VCI calculations, nonet and septet states have been considered, with the restriction that the antiferromagnetic coupling was allowed only for the two unpaired electrons of CO. In this way, we were able to investigate whether any topological difference between the a $^3\Pi$ and the A $^1\Pi$ states of the CO molecule interacting with the surface could be observed. It turned out that our approach in which we focus on the calculation of the a $^3\Pi$-like state was justified since the topologies of the PESs for a $^3\Pi$ and A $^1\Pi$ were essentially identical.

The CO bond distance was chosen to be 1.128 Å, which is the experimental value of the equilibrium distance in the electronic ground state of the molecule in the gas phase.[21] We will include the internal CO vibration in our future studies in order to check the quality of the calculated PES with frozen CO distance. Nevertheless, our calculations for CO in the gas phase show that the CO bond distance changes after the $5\sigma \rightarrow 2\pi^*$ excitation only by ≈0.06 Å. Therefore, it is reasonable that such a small change of the CO bond distance should only slightly influence the topology of the calculated PES.

All calculations have been performed using the Bochum suite of ab initio programs.[26−29] We used triple-$\zeta$ basis sets of Huzinaga $(9s\ 5p) \rightarrow \langle 6s\ 3p\rangle$[30,31] for CO and the oxygen atoms of the cluster and a Wachters basis set $(14sp\ 5d) \rightarrow \langle 9s\ 6p\ 4d\rangle$[32] for chromium. The original set of Wachters was augmented by an additional s-function ($\eta = 0.24877$) in order to close the gap between the 3s and 4s orbitals. Furthermore, d-polarization functions have been added to the Huzinaga basis sets for CO (two d functions for each atom, carbon and oxygen). The details of these basis sets are collected in Table 1.

Because of the incomplete basis sets, the calculated interaction energies have to be corrected for the basis set superposition error (BSSE). For the ground state, we applied the well-known counterpoise correction scheme of Boys and Bernardi,[33] which

requires the use of the whole basis set to calculate the energy of the whole system as well as that of the separated fragments. In the present study, we consider the excited state of the CO molecule. In this case, care is needed when applying the counterpoise correction (see for instance the discussion in ref 34). We assume that the BSSE of the CO molecule is the same both in the ground and in the excited state (which is not exactly true, though) and will use the energy of the nonexcited CO molecule in the whole basis set for the counterpoise correction. The interaction energy is then given by:

$$\Delta E = E^{\mathrm{wb}}(\mathrm{CO}(\mathrm{a}\,^3\Pi), \mathrm{cluster}) - E^{\mathrm{wb}}(\mathrm{cluster}) - E^{\mathrm{wb}}(\mathrm{CO}(\mathrm{X}\,^1\Sigma^+))$$

where wb, whole basis, indicates the use of the whole basis to calculate all three energy contributions.

The fairly large basis set used for the CO molecule causes a very small contribution to the whole BSSE anyway, so that the error introduced by our modified counterpoise scheme is small as compared to the interaction energies and can be neglected.

We have calculated 4410 data points according to the following sampling pattern: 10 points in the $Z$ coordinate (between 3.0 and 7.0 au with an increment of 0.5 au and one point at 10.0 au), seven points on the $X$-axis (0.0 au, from 2.5 to 7.5 au with an increment of 1.0 au), the values for the tilt angle $\vartheta$ were varied between 0 and 180° with an increment of 22.5°, the angle $\varphi$ was varied in the same region with an increment of 30°, whereby we assume a mirror symmetry of the PES with respect to the $\varphi$ coordinate: a rotation between 360 and 180° is the same as a rotation between 0 and 180°. (At some points with small $Z$ values ($<$4.0 au), it was difficult to reach convergence of the CASSCF calculations. In these cases, we estimated the energy by 1D interpolations using neighboring data points for larger $Z$ (or sometimes for the same $Z$ but for different $\vartheta$ or $\varphi$ values), which were well-converged. At most, 100 data points were constructed by this procedure; all others were taken from the real calculations.)

**2.5. Fitting Procedure.** For the subsequent wave packet calculations, it was necessary to construct an analytic function, which represents the calculated PES. We will briefly describe the fitting procedure that we have applied.

The following function was used

$$f = u_0 + u_1/z^3 + u_2/z^4 + u_3 \exp(-u_4(z - u_5)^2)$$

where

$$u_i = \sum_{j=0}^{3} v_{ji} \cos(j\varphi), \text{ for } i \neq 0$$

and

$$v_{ji} = \sum_{k=0}^{2} a_{kji} \cos(k\vartheta) + \sum_{k=1}^{2} b_{kji} \sin(k\vartheta), \text{ for } j = 0$$

$$v_{ji} = \sum_{k=1}^{2} c_{kji} \sin(k\vartheta), \text{ for } j \neq 0$$

where $u_0$, $a_{kji}$, $b_{kji}$, and $c_{kji}$ are functions of $\alpha = 2\pi X/a_0$ ($a_0$ lattice constant), which is the periodic $X$ coordinate

$$u_0 = \sum_{m=0}^{2} p_{m0} \cos(m\alpha) + \sum_{m=1}^{2} q_{m0} \sin(m\alpha)$$

$$a_{kji} = \sum_{m=0}^{2} s_{mkji} \cos(m\alpha) + \sum_{m=1}^{2} t_{mkji} \sin(m\alpha)$$

and corresponding expressions for $b_{kji}$ and $c_{kji}$.

In general, the fit function consists of Fourier-like expansions in the coordinates $\vartheta$ and $\varphi$ as well as in $X$, which are coupled to the $Z$-dependent terms and to each other. The amplitudes of the Fourier expansions were treated as adjustable parameters $p$, $q$, $s$, and $t$ (and others not shown here explicitly; in total, there are 280 parameters in the present fit function; parameters are available on request).

We use the standard Levenberg−Marquardt algorithm[35] to fit the adjustable parameters of our fit function to the calculated data points. The calculated interaction energies between the excited CO molecule and the surface cover a large range of many orders of magnitude (from about −60 kJ/mol up to +2000 kJ/mol). The negative values, which correspond to the attractive interaction, are very small as compared to the large positive values in the repulsive regions of the PES. To obtain a good description of those regions of the PES that are of importance for the desorption process, we have applied a special weighting scheme, which ensures a preferential treatment of the data points close to the absolute energy minimum of the PES (−30 to −60 kJ/mol). This was done by setting the weight for different data points according to the Boltzmann distribution $\exp(-\Delta E/kT)$, where $\Delta E = E_i - E_{\min}$ is the energy difference between the data point $i$ and the absolute minimum of the PES. The value for $kT$ was chosen to be 150 kJ/mol, which is large enough to ensure large weights for data points with interaction energies up to +50 kJ/mol.

However, this weighting scheme neglects the data points with very strong repulsive interaction ($E$ > 500 kJ/mol) almost completely. This is not always desired, because the strongly repulsive interaction occurs mostly at small binding distances. As we have to construct an analytic function with the correct physical behavior at any binding distance, we cannot use very small weights for data points in the repulsive region of the PES. Therefore, we have substituted the estimated Boltzmann weight factors for data points for smallest binding distances ($Z$ = 3.0 au) by 0.33. This was done for data points with $Z$ = 10.0 au as well. In this way, we accurately represent three regions on the whole PES: close to the absolute minimum and asymptotic regions at both large and small binding distances. Using this weighting scheme, we were able to construct an analytic fit function, which describes well the binding region of the PES and shows a correct physical behavior in the asymptotic regions.

## 3. Results and Discussion

**3.1. Topology of the Calculated 4D PES.** A complete 4D PES $f(X, Z, \vartheta, \varphi)$ for the interaction of the excited CO molecule ($a\,^3\Pi$) with the surface has been calculated in the present study (we will also use the CO* symbol to indicate the CO molecule in the $a\,^3\Pi$ state). The number of the calculated data points (4410) is large enough to describe all possible orientations of the CO molecule at all possible positions between two neighboring Cr ions above the surface with a sufficient accuracy. The main features of the topology of the calculated 4D PES can be seen in a 2D representation where (see Figure 3) only

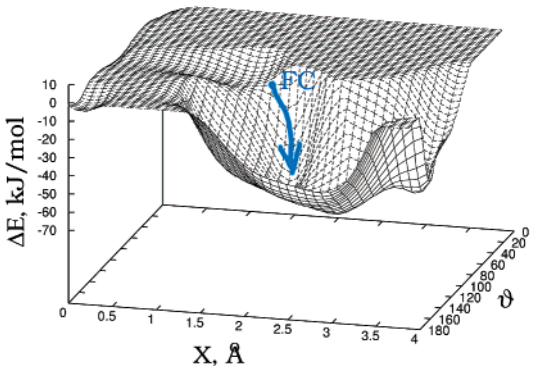


**Figure 3.** 2D representation of the 4D PES for CO* at the $Cr_2O_3$ (0001) surface. "FC" indicates the Franck−Condon region. The arrow symbolizes the probable evolution pathway of a wave packet on the exited state PES.

the $X$ and $\vartheta$ coordinates are shown explicitly while $Z$ and $\varphi$ have been optimized, i.e., every point $E(X,\vartheta)$ is the minimum on the $(Z,\varphi)$ PES cut for given values $X$ and $\vartheta$.

A large flat area at $\vartheta < 90°$ corresponds to the purely repulsive interaction of CO* with the surface. The optimization of the $Z$ and $\varphi$ coordinates was performed starting from large $Z$ values at which no interaction of the CO molecule with the surface occurs. Because of the pure repulsive interaction in some regions of the PES, the starting energy values that were zero did not get smaller when the CO molecule approached the surface. This is the reason for the large flat area in the 2D representation of the calculated 4D PES, which should be considered as an artifact of the illustration.

There is a ravinelike minimum at large $\vartheta$ values (between 150 and 180°). Thus, at the minimum of the PES, the CO* molecule is oriented almost perpendicular to the surface with the carbon atom down. It is remarkable that tilting of the CO molecule ($\vartheta \approx 160°$) varies only slightly in the range of $X$ values between 1.5 and 3.0 Å, and also, the interaction energy remains almost unchanged in this region (it varies only between 58 and 55 kJ/mol). This is mainly due to the interaction of the quadrupole moment of CO* with the electric field gradient at the surface. This will be discussed in detail in the next subsection.

Furthermore, a more detailed analysis of the available data indicates that the interaction energy is quite independent of $\varphi$. This is not surprising for a CO molecule, which is just slightly tilted with respect to the surface normal.

The value of the binding energy in the minimum is 58 kJ/mol, which is rather large as compared to the calculated value of 27 kJ/mol for the ground state.[8] This increase of the interaction energy for CO* is mainly due to the change in the occupation of the $5\sigma$ and $2\pi^*$ orbitals: it causes reduction of the Pauli repulsion due to the missing electron in the $5\sigma$ orbital as well as an increased polarization of CO* in the surface field due to the occupation of the diffuse $2\pi^*$ orbitals.

We want to pay a little more attention to the most important regions of the calculated PES. The first step of a DIET process may be very roughly imagined as a time propagation of the wave packet on the PES of the intermediate state after the transition (usually Franck−Condon transition) from the equilibrium position of the ground state. The Franck−Condon region of our system is indicated by "FC" in Figure 3. This point is just "on the way" from the repulsive region of the PES to its minimum. Most probably, the wave packet will "move" into the minimum (as indicated by the arrow). The corresponding changes of the CO coordinates would be probably as follows: $\vartheta$ will become larger as well as $X$; however, it is not obvious from Figure 3 what will happen with two others coordinates $Z$ and $\varphi$; a detailed discussion will be given in a future publication.[36]

This oversimplified picture is useful to show that only the part of PES "between" the FC point and the minimum will be important for the dynamics. This region of the PES covers the binding energy range between −20 and −60 kJ/mol. That is the reason for adjusting the fitting procedure in the way that it favors exactly this region of the PES (as well as both asymptotic regions at large and small binding distances to ensure a physically correct behavior of the fit function).

**TABLE 2: Calculated Values for the Bound Distances and for the Dipole and Quadrupole Moment of CO in the Ground $X^1\Sigma^+$ and the Excited a $^3\Pi$ and A $^1\Pi$ States (Referring to the Center of Mass of CO**

| | SCF | CASSCF | |
|---|---|---|---|
| moments | X $^1\Sigma^+$ | a $^3\Pi$ | A $^1\Pi$ |
| $R_e$ (Å) | 1.104 | 1.169 | 1.195 |
| $\mu$ (au) | 0.101 | 0.776 | 0.533 |
| $\Theta_{xx}$ (au) | 0.758 | −1.218[a] | −1.396[a] |
| $\Theta_{yy}$ (au) | 0.758 | 0.766[a] | 0.822[a] |
| $\Theta_{zz}$ (au) | −1.516 | 0.452 | 0.575 |

[a] For the spacially 2-fold degenerate $\Pi$ states, two sets of $\Theta_{xx}$ and $\Theta_{yy}$ exist although not explicitly given here. These values are related by the equations $\Theta_{xx}^{(1)} = \Theta_{yy}^{(2)}$ and $\Theta_{yy}^{(1)} = \Theta_{xx}^{(2)}$ where (1) and (2) indicate different spacial components.

**3.2. Interaction Mechanism.** The orientation of the excited CO molecule at the surface is determined mainly by the interplay of electrostatic attraction and Pauli repulsion. Similar to the situation in the ground state of this system,[8] the quadrupole moment of CO (rather than the dipole moment) dominates the electrostatic interaction. The calculated values for diagonal elements of the quadrupole moment tensor as well as for the dipole moment of the isolated CO molecule in the ground $X\ ^1\Sigma^+$ and the first excited a $^3\Pi$ states are given in the Table 2.

While in the X $^1\Sigma^+$ ground state the symmetry of the quadrupole moment tensor resembles that of the $d_{z^2}$ orbital (and $|\Theta_{zz}| > |\Theta_{yy}|$), the situation changes in the excited a $^3\Pi$ state: the spatially degenerate state gives rise to two different sets of $\Theta_{xx}$ and $\Theta_{yy}$ values, which have absolute values larger than $\Theta_{zz}$. One may combine the diagonal elements of the quadrupole moment tensor $\Theta$ to "+" and "−" linear combinations (LC). The resulting − LC will possess the symmetry of pure $d_{x^2-y^2}$ orbital, while the + LC will resemble the symmetry of the $d_{z^2}$ orbital (like in the ground state but with the opposite sign). Thus, the excitation of the CO molecule is accompanied by change of the symmetry of its quadrupole moment from $d_{z^2}$-like to the $d_{x^2-y^2}$-like or with the change of the sign of the poles of $\Theta$ from prolate to oblate.

We can verify this picture using a very simple model system $Li^+$/CO. Let us compare the interaction of a lithium cation with a CO molecule in the ground and the first excited states for linear and T-like arrangements (see Figure 4). It was already shown by Staemmler[37] that the CO molecule in its ground state prefers the linear arrangement with $Li^+$ (due to lone pairs at carbon and oxygen atoms or the prolate negative quadrupole moment, which dominates the interaction). In contrast, the interaction of $Li^+$ with the excited CO molecule (a $^3\Pi$) is stronger for T-like arrangements. This is easy to understand, because $\Theta$ is now oblate and negative. (Two different curves for the T-like complex are due to the two components of the $^3\Pi$ state with different values for $\Theta_{xx}$ and $\Theta_{yy}$.) This simplified model clearly demonstrates the dominant role of the quadrupole

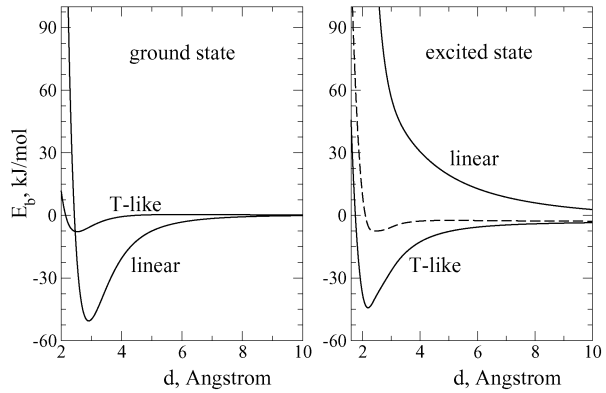


**Figure 4.** Potential curves for the interaction of $Li^+$ with the CO molecule in the ground (left) and excited (right) state (the dashed line on the right picture corresponds to the upper state of the T-like species).

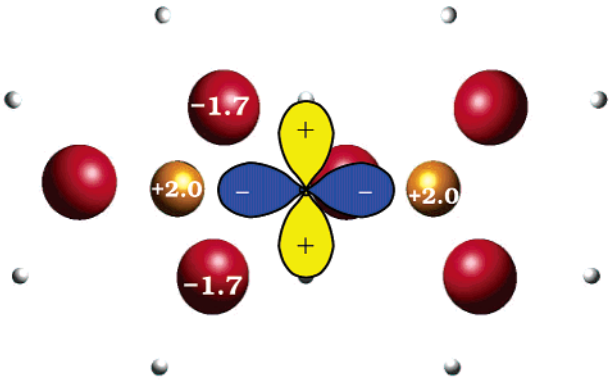


**Figure 5.** Schematic representation of the interaction of the quadrupole moment of CO* with the $Cr_2O_3$ (0001) surface.

moment of CO (a $^3\Pi$), even though the dipole moment becomes larger than in the ground state.

Concerning the interaction of the excited CO molecule with the $Cr_2O_3$ (0001) surface, it can be rationalized how the $d_{x^2-y^2}$-like quadrupole moment determines the orientation of the molecule. If CO* is placed between two adjacent chromium ions and is perpendicular to the surface, attractive interaction is found. In this position, the negative poles of the quadrupole moment are directed straight toward the two chromium ions while the interaction of the positive poles with chromium ions is avoided (one may also assume that there is some attraction between the positive poles and the oxygen ions; see Figure 5). Furthermore, CO* has a quite diffuse electron distribution and interacts with both chromium ions simultaneously. Therefore, the minimum on the calculated PES is quite broad along the *X* coordinate.

Finally, the carbon-down orientation is more favorable, because the 5$\sigma$ orbital (the lone electron pair at the carbon site) is occupied by just one electron so that the Pauli repulsion is much smaller as it would be in the case where the oxygen atom with its doubly occupied lone pair is closer to the surface.

**3.3. Splitting of the a $^3\Pi$ States of CO at the Surface.** The a $^3\Pi$ state of CO is degenerate in the gas phase. However, the two spatial components are not exactly equal any more at the surface. The extent of their splitting depends on the orientation of the adsorbed molecule. In this situation, it is not obvious whether state-averaged CASSCF calculations are justified for every CO orientation. Alternatively, a single reference SCF calculation for the lower lying component of the a $^3\Pi$ state could have been preferable.

We have decided to apply the uniform calculation scheme (state-averaged CASSCF calculation for both spacial components of the a $^3\Pi$ state) for any CO orientation and at any adsorption distance. We are interested in the complete PES and not in some special regions only. A uniform treatment of the whole coordinate space seemed to be more appropriate in order to avoid steps or kinks within the calculated PES. At the same time, we have avoided SCF convergence problems, which were observed for regions with small splitting of the a $^3\Pi$ state.

The error induced by applying state-averaged CASSCF is expected to be small in the most important regions of the PES: the region that corresponds to the minimum of the ground state PES, i.e., the Franck−Condon region, the minimum region of the calculated PES for the excited state and the regions between these two. The splitting of the a $^3\Pi$ state in the Franck−Condon region is 12.7 kJ/mol in the state-averaged CASSCF calculation and 20.7 kJ/mol if both components are optimized in separate SCF calculations. At the PES minimum, we obtain 28.8 and 33.7 kJ/mol, respectively. The error due to the state-averaged CASSCF calculation is only 8 kJ/mol in the Franck−Condon region and is even smaller (∼5 kJ/mol) in the region of the minimum. This error is also small for other areas of the calculated PES, as we could see from a detailed analysis of our data. Although this error is not constant over the whole calculated PES, it is small enough to be neglected, especially if we keep in mind the question, which of both components of the a $^3\Pi$ state has to be optimized at different positions and orientations of the excited CO molecule at the surface (these difficulties make an efficient calculation of the 4D PES impossible).

**3.4. Separation between the a $^3\Pi$ and A $^1\Pi$ States of CO at the Surface.** In Section 2, we have decided to consider the a $^3\Pi$ state as a desorption intermediate. However, it is necessary to consider the A $^1\Pi$ state as well. To show that no major differences between these two states exist with respect to the interaction with the surface, we have evaluated the energy separation between the $^3\Pi$- and the $^1\Pi$-like states from the VCI calculations. It is clear that at large adsorption distances this separation is the same as in the gas phase and changes when the molecule approaches the surface. The change of the $^3\Pi-{}^1\Pi$ energy separation might be different for different orientations of the adsorbed molecule. We again will consider only two positions on the calculated PES: its minimum and the Franck−Condon region (which corresponds to the minimum on the ground state PES).

Figure 6 shows a plot of the $^3\Pi-{}^1\Pi$ energy separation as a function of the *Z* coordinate for two adsorption sites of the calculated PES: at the minimum and in the Franck−Condon region (we keep the orientation of the CO molecule and its lateral position above the surface according to the respective geometry and vary only the *Z* coordinate). For both orientations of the CO* molecule, the curves are almost identical and *Z*-independent at $Z > 3.5$ Å. At smaller adsorption distances, the separation is decreasing by 0.1−0.2 eV, and only when the CO molecule gets quite close to the surface ($Z < 2.5$ Å), the singlet−triplet separation changes remarkably. Thus, for intermediate and large adsorption distances, the interaction of the excited CO molecule with the surface is similar for both spin orientations of the excited electron. This is in accordance with the fact that the symmetry and the values of the quadrupole moment in both states, $^3\Pi$ and $^1\Pi$, are very similar to each other (see Table 2). The deviations from this behavior at small *Z* distances are probably due to the different polarizabilities of the CO molecule in the triplet a $^3\Pi$ and singlet A $^1\Pi$ states.

Thus, the calculated PES for the interaction of the CO molecule in the a $^3\Pi$ state with the surface describes the most

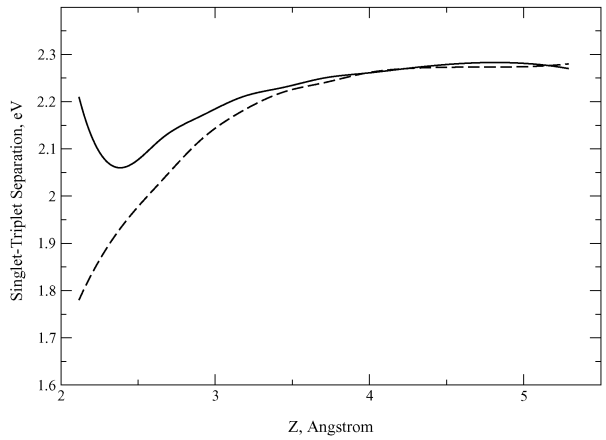


**Figure 6.** Singlet−triplet energy separation for two particular CO adsorption sites: the Franck−Condon region (solid line) and the minimum of the calculated PES (dashed line).

important electrostatic component correctly, and we do not expect any crucial deviations between the tripletlike and the singletlike states. Therefore, it is irrelevant whether the dipole forbidden triplet or the dipole allowed singlet state is considered to be the desorption intermediate. The interaction energies and the topology of the two PESs should be very similar.

## 4. Conclusions

We have presented ab initio calculations of the 4D PES for an excited state of the adsorbate−substrate system $CO/Cr_2O_3$ (0001). An internal excitation of the CO molecule ($5\sigma \rightarrow 2\pi^*$) was assumed to generate the intermediate state involved in the photoinduced desorption. The calculation has been performed for the $^3\Pi$-like state even though the transition to this state from the $X\ ^1\Sigma^+$ ground state is dipole forbidden.

The topology of the calculated PES for the excited state differs remarkably from that of the ground state. We explain the topology of the PES for the excited state mainly by the interaction of the quadrupole moment of the excited CO molecule with the electric field gradient of the surface. We also discuss the reliability of the chosen a $^3\Pi$ state as a desorption intermediate and explain why a similar PES should result also for the A $^1\Pi$ state.

We also present the fit technique that was successfully applied to construct an analytic function, which represents the calculated 4D PES. This fit function was already used for the subsequent wave packet calculations presented elsewhere.[9,14]

The calculated PES (together with the PES for the electronic ground state) is the crucial input for a subsequent quantum dynamical treatment of DIET phenomena beyond empirical, low-dimensional models. Therefore, the present study is the foundation for a detailed mechanistic insight into photochemical reactions for the $CO/Cr_2O_3$ (0001) adsorbate−substrate system.

**Acknowledgment.** We are grateful to the Deutsche Forschungsgemeinschaft for the financial support through the Schwerpunktprogramm DFG-SPP1093 "Dynamik von Elektronentransferprozessen an Grenzflächen". We thank Prof. Dr. H.-J. Freund and Dr. H. Kuhlenbeck for helpful discussions. We also thank Prof. Dr. V. Staemmler for many helpful suggestions and carefully reading the manuscript.

## References and Notes

(1) Kuhlenbeck, H.; Xu, C.; Dillmann, B.; Haβel, M.; Adam, B.; Ehrlich, D.; Wohlrab, S.; Freund, H.-J.; Ditzinger, U.; Neddermeyer, H.; Neuber, M.; Neumann, M. *Ber. Bunsen-Ges. Phys. Chem.* **1992**, *96*, 15.
(2) Scarano, D.; Zecchina, A.; Bordiga, S.; Ricchiardi, G.; Spoto, G. *Chem. Phys.* **1993**, *177*, 547.
(3) Zecchina, A.; Scarano, D.; Bordiga, S.; Ricchiardi, G.; Spoto, G.; Geobaldo, F. *Catal. Today* **1996**, *27*, 403.
(4) Xu, C.; Dillmann, B.; Kuhlenbeck, H.; Freund, H.-J. *Phys. Rev. Lett.* **1991**, *67*, 3551.
(5) Freund, H.-J.; Kuhlenbeck, H.; Staemmler, V. *Rep. Prog. Phys.* **1996**, *59*, 283.
(6) Beauport, I.; Al-Shamery, K.; Freund, H.-J. *Chem. Phys. Lett.* **1996**, *256*, 641.
(7) Henrich, V.; Cox, P. *The Surface Science of Metal Oxides*; Cambridge University Press: Cambridge, 1994.
(8) Pykavy, M.; Staemmler, V.; Seiferth, O.; Freund, H.-J. *Surf. Sci.* **2001**, *479*, 11.
(9) Thiel, S.; Pykavy, M.; Klüner, T.; Freund, H.-J.; Kosloff, R.; Staemmler, V. *Phys. Rev. Lett.* **2001**, *87*, 077601.
(10) Menzel, D.; Gomer, R. *J. Chem. Phys.* **1964**, *41*, 3311.
(11) Readhead, P. *Can. J. Phys.* **1964**, *42*, 886.
(12) Antoniewicz, P. *Phys. Rev. B* **1980**, *21*, 3811.
(13) Klüner, T.; Freund, H.-J.; Staemmler, V.; Kosloff, R. *Phys. Rev. Lett.* **1998**, *80*, 5208.
(14) Thiel, S.; Pykavy, M.; Klüner, T.; Freund, H.-J.; Kosloff, R.; Staemmler, V. *J. Chem. Phys.* **2002**, *116*, 762.
(15) Wyckoff, R. *Crystal Structures*, 2nd ed.; Wiley: New York, 1964; Vol. II.
(16) Rohr, F.; Bäumer, M.; Freund, H.-J.; Mejias, J.; Staemmler, V.; Müller, S.; Hammer, L.; Heinz, K. *Surf. Sci.* **1997**, *372*, L291.
(17) Rohr, F.; Bäumer, M.; Freund, H.-J.; Mejias, J.; Staemmler, V.; Müller, S.; Hammer, L.; Heinz, K. *Surf. Sci.* **1997**, *389*, 391.
(18) Rehbein, C.; Harrison, N.; Wander, A. *Phys. Rev. B* **1996**, *54*, 14066.
(19) Leitheuβer, A. *Periodische Hartree−Fock-Rechnungen an Oxidoberfächen*, Ph.D. Thesis, Ruhr-Universität Bochum, 1999.
(20) Mejias, J.; Staemmler, V.; Freund, H.-J. *J. Phys. C: Condens. Matter* **1999**, *11*, 7881.
(21) Huber, K.; Herzberg, G. Constants of Diatomic Molecules; data prepared by Gallagher, J. W.; Johnson, R. D., III. In *NIST Chemistry WebBook: NIST Standard Reference Database Number 69*; Linstrom, P. J.; Mallard, W. G., Eds.; National Institute of Standards and Technology: Gaithersburg, MD, 2001; http://webbook.nist.gov.
(22) Refaey, K.; Franklin, J. *Int. J. Mass Spectrom. Ion Phys.* **1976**, *20*, 19.
(23) Ferrari, A.; Pacchioni, G. *J. Chem. Phys.* **1997**, *107*, 2066.
(24) Erman, P.; Karawajczyk, A.; Rachlew-Kallne, E.; Stromholm, C.; Larsson, J.; Persson, A.; Zerne, R. *Chem. Phys. Lett.* **1993**, *215*, 173.
(25) Samuelsen, E.; Hutchungs, M.; Shirane, G. *Physica* **1970**, *48*, 13.
(26) Staemmler, V. *Theor. Chim. Acta* **1977**, *45*, 89.
(27) Meier, U.; Staemmler, V. *Theor. Chim. Acta* **1989**, *76*, 95.
(28) Wasilewski, J. *Int. J. Quantum Chem.* **1989**, *36*, 503.
(29) Fink, R.; Staemmler, V. *Theor. Chim. Acta* **1993**, *87*, 129.
(30) Huzinaga, S. *Approximate Atomic Functions I*; Technical Report; University of Alberta: Canada, 1971.
(31) Huzinaga, S. *J. Chem. Phys.* **1965**, *42*, 1293.
(32) Wachters, A. *J. Chem. Phys.* **1970**, *52*, 1033.
(33) Boys, S.; Bernardi, F. *Mol. Phys.* **1970**, *19*, 553.
(34) van Duijneveldt, F.; van Duijneveldt-van de Rijdt, J.; van Lenthe, J. *Chem. Rev.* **1994**, *94*, 1873.
(35) Press, W.; Teukolsky, S.; Vetterling, W.; Flannery, B. *Numerical Recepies in Fortran: The Art of Scientific Computing*, 2nd ed.; Cambridge University Press: New York, 1992.
(36) Borowski, S.; Klüner, T. To be published.
(37) Staemmler, V. *Chem. Phys.* **1976**, *17*, 187.